



# Robust Direction-Finding Method for Sensor Gain and Phase Uncertainties in Non-uniform Environment

Long Yang<sup>1</sup> · Yixin Yang<sup>2</sup> · Guisheng Liao<sup>1</sup> · Yong Wang<sup>2</sup>

Received: 24 May 2018 / Revised: 9 August 2019 / Accepted: 10 August 2019 / Published online: 23 August 2019  
© Springer Science+Business Media, LLC, part of Springer Nature 2019

## Abstract

A direction-of-arrival (DOA) estimation algorithm, which is robust to sensor gain and phase uncertainties for completely uncalibrated arrays in a non-uniform noise environment, is proposed in this study. As a result of the sensor gain uncertainties or the shielding effects for some baffled arrays, the noise power may vary with sensors. Therefore, a non-uniform noise model is considered. A cost function established by the orthogonality of subspaces is accumulated along several rough space intervals surrounding the real angles of sources. After analyzing the influences of rough space intervals, an iterative refinement operation is carried out to improve the estimation performance of the DOA and sensor gain and phase responses. The Cramér–Rao bounds of the DOA and sensor gain and phase in the non-uniform noise model are derived. Simulations and experimental results show the superiority of the proposed method.

**Keywords** Self-calibration · Robust DOA estimation · Sensor gain and phase uncertainties · Uncalibrated arrays

---

✉ Yixin Yang  
yxyang@nwpu.edu.cn

Long Yang  
ylong311@126.com

Guisheng Liao  
liaogs@xidian.edu.cn

Yong Wang  
yongwang@nwpu.edu.cn

<sup>1</sup> National Laboratory of Radar Signal Processing, Xidian University, Xi'an 710071, Shaanxi, China

<sup>2</sup> School of Marine Science and Technology, Northwestern Polytechnical University, Xi'an 710072, China

## 1 Introduction

Direction-of-arrival (DOA) estimation is an important task in underwater acoustic signal processing [11, 16, 27]. Eigenstructure-based direction-finding techniques (e.g., multiple signal classification (MUSIC) [15], estimation of signal parameters via rotational invariance techniques (ESPRIT) [14], and weighted subspace fitting [18]) can achieve a high resolution when ideal arrays without any model mismatch are considered. However, both signal and noise model mismatches degrade the performance of DOA estimation, particularly in terms of the resolution ability and location accuracy. Most applications have assembled sensors in fixed positions that can be measured or well calibrated beforehand [3, 21]. However, the gain and phase uncertainties are difficult to compensate, especially when the responses of sensors change with the environment.

Self-calibration is a useful technique for uncalibrated arrays to provide the robust DOA estimations [1, 2, 17, 22–24, 26, 29]. Friedlander and Weiss [22] applied an iterative procedure to find the minimum of a cost function to compensate for sensor gain and phase perturbations and estimate the unknown DOA. However, the initial value of the iterative procedure seriously influences the performance of parameter estimation, and the global minimum is hard to achieve. Then, Zhang and Zhu [29] proposed a similar cost function in some rough space intervals of the real DOA of sources to calibrate sensor gain and phase parameters. However, the large range of rough space intervals degrades the accuracy of parameter estimation.

Another type of robust direction-finding technique focuses on DOA estimation with partly calibrated sensor arrays [6–8, 12, 19, 20, 30]. The ESPRIT-like algorithm [7] was proposed to achieve DOA estimation and calibrate sensor gain and phase parameters with partly calibrated arrays exhibiting a rotational invariance structure. A satisfactory DOA estimation can be obtained when at least two sensors are calibrated. For quasi-stationary signals, an underdetermined DOA estimation method is proposed by using the idea of ESPRIT-like algorithm in partly calibrated arrays [19]. In fully using the aperture of arrays, an improved ESPRIT-like algorithm [8] can approach the Cramér–Rao bounds (CRBs). Although these ESPRIT-like-based self-calibration algorithms [7, 8, 19] can estimate DOA and sensor responses robustly, their applications are still limited due to the rotational invariance of array structures. For complex situations where the indices of the partly calibrated sensors are unknown and the array shape is arbitrary, a compressive sensing-based robust DOA estimation method [20] is proposed, and the miscalibrated sensors can be eliminated with adaptive weights on the basis of maximum correntropy criterion. However, it only applies to the case that only a few sensors are miscalibrated.

Noise model mismatch is another factor to degrade DOA estimation performances [4, 9, 10, 25, 27, 28]. In some applications (e.g., the shielding effects for some baffled arrays), the powers of additive noises are not uniform along the sensor array; thus, the non-uniform noise model is widely studied [4, 9, 10, 28]. The influence on the non-uniform noise power can be removed by considering the non-diagonal elements in the covariance matrix. Hence, a kind of DOA estimation algorithms in non-uniform noise environment is achieved [4, 9, 28]. Considering the parameterized covariance matrix, an iterative algorithm for subspace estimation by maximizing the log-likelihood func-

tion is proposed [10]. Combined with the ESPRIT-like algorithm, a subspace-based DOA estimation method for partly calibrated arrays in non-uniform noise is obtained [10].

In the field of sensor gain and phase calibrations, there are still some difficulties to be solved, such as the global convergence problem for the iteration-based algorithms, the requirement of partly calibrated sensors and the non-uniformity of additive noise. To solve these problems, a robust DOA estimation algorithm for sensor gain and phase uncertainties with completely uncalibrated arrays is proposed. The signal subspace of the covariance matrix in the non-uniform noise environment is first estimated. To achieve the global convergence, a robust initialization is calculated by solving a cost function which is established by the orthogonality of subspaces and accumulated along several rough space intervals surrounding the real directions of sources. Then, an iterative refinement operation is carried out to improve the estimation performance of the DOA and the sensor gain and phase responses. In this manner, no partly calibrated sensor is required. In addition, the CRBs of the DOA and sensor gain and phase in the non-uniform noise model are derived. Simulation results showed that the proposed method can estimate the DOA of sources and sensor responses precisely in comparison with the CRBs. The effectiveness of the proposed method is also confirmed by experimental results in an anechoic tank with a baffled uniform circular array (UCA).

## 2 Signal Model

Consider an array composed of  $M$  sensors with half-wavelength inter-element spacing.  $K$  narrowband and uncorrelated signals impinge on the array from the far field. The array observation vector  $\mathbf{x}(n)$  at the  $n$ th snapshot is modeled as follows:

$$\mathbf{x}(n) = \text{diag}\{\boldsymbol{\gamma}\} \mathbf{A}(\boldsymbol{\theta}) \mathbf{s}(n) + \mathbf{e}(n), \quad (1)$$

where  $\mathbf{A}(\boldsymbol{\theta}) = [\mathbf{a}(\theta_1), \mathbf{a}(\theta_2), \dots, \mathbf{a}(\theta_K)]$  is the  $M \times K$  nominal steering matrix when dealing with the absence of gain and phase perturbations;  $\mathbf{a}(\theta_k)$  is the  $M \times 1$  nominal steering vector of the  $k$ th signal;  $\boldsymbol{\theta} = [\theta_1, \dots, \theta_K]^T$  is the DOA of received signals.  $\mathbf{s}(n)$  and  $\mathbf{e}(n)$  are the statistically independent waveforms of signals and noise, respectively, and  $\text{diag}\{\boldsymbol{\gamma}\}$  is a diagonal matrix of the bracketed vector  $\boldsymbol{\gamma}$ , which denotes the sensor gain and phase parameters. We assume that all sensor gain and phase parameters are unknown and direction independent [7]. Then, the parameter  $\boldsymbol{\gamma}$  can be modeled as follows:

$$\boldsymbol{\gamma} = [\gamma_1, \gamma_2, \dots, \gamma_M]^T, \quad (2)$$

where  $\gamma_m = g_m e^{j\varphi_m}$ ;  $g_m$  and  $\varphi_m$  are the sensor gain and phase responses, respectively; and  $\gamma_1$  is generally equal to 1 for unique identification [22].

Considering the non-uniformity of sensor responses, especially for hydrophones in an underwater environment, we utilize a non-uniform noise model applied as a non-

uniform and uncorrelated zero-mean Gaussian process. Then, the data covariance matrix  $\mathbf{R}$  is given by the following:

$$\mathbf{R} = \text{diag}(\boldsymbol{\gamma})\mathbf{A}(\boldsymbol{\theta})\mathbf{P}\mathbf{A}^H(\boldsymbol{\theta})\text{diag}^H(\boldsymbol{\gamma}) + \mathbf{Q}, \quad (3)$$

where the noise covariance  $\mathbf{Q} = \text{diag}(\boldsymbol{\sigma})$ ;  $\mathbf{P} = \text{diag}\{\mathbf{p}\}$ ;  $\mathbf{p}$  and  $\boldsymbol{\sigma}$  denote the power of the signals and the non-uniform noises, respectively; and  $(\cdot)^H$  is the conjugate transpose. When  $N$  snapshots are available, the data covariance matrix can be calculated by the sample covariance matrix as  $\hat{\mathbf{R}} = 1/N \sum_{n=1}^N \mathbf{x}(n)\mathbf{x}^H(n)$ .

The signal covariance matrix  $\mathbf{P}$  in (2) is a full rank diagonal matrix, which can be decomposed as  $\mathbf{P} = \mathbf{T}\mathbf{T}^H$  and  $\mathbf{T}$  is a  $K \times K$  nonsingular matrix. Then the data covariance matrix  $\mathbf{R}$  in (3) can be reformulated as follows:

$$\begin{aligned} \mathbf{R} &= \text{diag}(\boldsymbol{\gamma})\mathbf{A}(\boldsymbol{\theta})\mathbf{T}\mathbf{T}^H\mathbf{A}^H(\boldsymbol{\theta})\text{diag}^H(\boldsymbol{\gamma}) + \mathbf{Q} \\ &= \mathbf{B}_s\mathbf{B}_s^H + \mathbf{Q}, \end{aligned} \quad (4)$$

where  $\mathbf{B}_s = \text{diag}(\boldsymbol{\gamma})\mathbf{A}(\boldsymbol{\theta})\mathbf{T}$ . Hence, the matrix  $\mathbf{B}_s$  spans the same column space as the matrix  $\text{diag}(\boldsymbol{\gamma})\mathbf{A}(\boldsymbol{\theta})$  (i.e., signal subspace).

### 3 Robust DOA Estimation Method

In this section, we focus on the self-calibration technique in estimating sensor gain and phase responses and DOA of signals simultaneously.

#### 3.1 Cost Function for Robust DOA Estimation

The sensor gain and phase parameters are generally estimated by applying the orthogonality of signal and noise subspaces [17, 22–24, 29]. However, the solutions of the sensor gain and phase parameters are sensitive to the DOA of sources. To solve this problem, an optimization problem for self-calibration by integrating the orthogonal relationship on an interval around the DOA is formed as [29]

$$\begin{aligned} \min_{\boldsymbol{\gamma}} \sum_{k=1}^K \int_{\theta_{k,L}}^{\theta_{k,U}} \boldsymbol{\gamma}^H \text{diag}^H\{\mathbf{a}(\theta)\} \Pi_{\mathbf{B}_s} \text{diag}\{\mathbf{a}(\theta)\} \boldsymbol{\gamma} d\theta \quad \text{s.t. } \mathbf{e}_1^H \boldsymbol{\gamma} = 1 \\ \Leftrightarrow \min_{\boldsymbol{\gamma}} \boldsymbol{\gamma}^H \boldsymbol{\Gamma} \boldsymbol{\gamma} \quad \text{s.t. } \mathbf{e}_1^H \boldsymbol{\gamma} = 1, \end{aligned} \quad (5)$$

where the noise subspace is calculated as  $\Pi_{\mathbf{B}_s} = \mathbf{I} - \mathbf{B}_s(\mathbf{B}_s^H \mathbf{B}_s)^{-1} \mathbf{B}_s^H$ ;  $\mathbf{B}_s$  is the signal subspace in the non-uniform noise model in (4) which can be effectively estimated by an iterative method [10]; and  $\mathbf{e}_1$  is an  $M \times 1$  vector, with the first element equal to 1 and the other equal to 0. Several rough intervals obtained by low-resolution direction-finding methods such as conventional beamforming (CBF) are represented as  $\Theta = \bigcup_{k=1}^K [\theta_{k,L}, \theta_{k,U}]$ , where  $\theta_{k,U}$  and  $\theta_{k,L}$  are the upper and lower bounds of the

$k$ th region, respectively;  $K$  is the number of sources; and the matrix  $\Gamma$  is expressed as follows:

$$\Gamma = \sum_{k=1}^K \int_{\theta_{k,L}}^{\theta_{k,U}} \text{diag}^H\{\mathbf{a}(\theta)\} \Pi_{\mathbf{B}_s} \text{diag}\{\mathbf{a}(\theta)\} d\theta. \tag{6}$$

Hence, the result of the minimization problem in (5) can be easily solved as follows:

$$\hat{\mathbf{y}} = \Gamma^{-1} \mathbf{e}_1 / (\mathbf{e}_1^H \Gamma^{-1} \mathbf{e}_1). \tag{7}$$

### 3.2 Influence Analysis of Rough Space Intervals

The influence of rough space intervals is discussed as follows. First, we assume that the noise subspace of the data covariance matrix  $\mathbf{R}$  in (3) is expressed as  $\mathbf{B}_n = [\mathbf{b}_1, \dots, \mathbf{b}_{M-K}]$ , that is,  $\Pi_{\mathbf{B}_s} = \mathbf{B}_n \mathbf{B}_n^H = \sum_{m=1}^{M-K} \mathbf{b}_m \mathbf{b}_m^H$ . Therefore,  $\Gamma$  can be calculated as

$$\Gamma = \sum_{m=1}^{M-K} \text{diag}\{\mathbf{b}_m\} \mathbf{G} \text{diag}^H\{\mathbf{b}_m\}, \tag{8}$$

where  $\mathbf{G} = \sum_{k=1}^K \int_{\theta_{k,L}}^{\theta_{k,U}} \mathbf{a}^*(\theta) \mathbf{a}^T(\theta) d\theta$ .

Without loss of generality, we assume that  $K = 1$  and that the real DOA is  $\theta_0$ ; then,  $\mathbf{G} = \int_{\theta_L}^{\theta_U} \mathbf{a}^*(\theta) \mathbf{a}^T(\theta) d\theta$ . The steering vector can be expressed by the Taylor series expansion at the point of  $\theta_0$ , as follows:

$$\mathbf{a}(\theta) \approx \mathbf{a}_0 + \mathbf{D}_1(\theta - \theta_0) + \mathbf{D}_2(\theta - \theta_0)^2, \tag{9}$$

where  $\mathbf{a}_0 = \mathbf{a}(\theta_0)$ . The third- and higher-order terms of  $\theta - \theta_0$  are ignored, and the differential vectors  $\mathbf{D}_1 = \left. \frac{\partial \mathbf{a}(\theta)}{\partial \theta} \right|_{\theta=\theta_0}$  and  $\mathbf{D}_2 = \left. \frac{\partial^2 \mathbf{a}(\theta)}{2 \cdot \partial \theta^2} \right|_{\theta=\theta_0}$ . Then,  $\mathbf{G}$  can be formed as

$$\begin{aligned} \mathbf{G} &= \int_{\theta_L}^{\theta_U} [\mathbf{a}_0^* + \mathbf{D}_1^*(\theta - \theta_0) + \mathbf{D}_2^*(\theta - \theta_0)^2][\mathbf{a}_0^T + \mathbf{D}_1^T(\theta - \theta_0) + \mathbf{D}_2^T(\theta - \theta_0)^2] d\theta \\ &\approx \int_{\theta_L}^{\theta_U} \mathbf{a}_0^* \mathbf{a}_0^T + [\mathbf{a}_0^* \mathbf{D}_1^T + \mathbf{D}_1^* \mathbf{a}_0^T](\theta - \theta_0) + [\mathbf{a}_0^* \mathbf{D}_2^T + \mathbf{D}_1^* \mathbf{D}_1^T + \mathbf{D}_2^* \mathbf{a}_0^T](\theta - \theta_0)^2 d\theta \\ &= \alpha_1 \mathbf{a}_0^* \mathbf{a}_0^T + \alpha_2 [\mathbf{a}_0^* \mathbf{D}_1^T + \mathbf{D}_1^* \mathbf{a}_0^T] + \alpha_3 [\mathbf{a}_0^* \mathbf{D}_2^T + \mathbf{D}_1^* \mathbf{D}_1^T + \mathbf{D}_2^* \mathbf{a}_0^T], \end{aligned} \tag{10}$$

where the third and higher-order terms of  $\theta - \theta_0$  are also ignored. The coefficients  $\alpha_1$ ,  $\alpha_2$ , and  $\alpha_3$  can be expressed as follows:

$$\begin{aligned}
 \alpha_1 &= \theta_U - \theta_L \\
 \alpha_2 &= \alpha_1[(\theta_U + \theta_L)/2 - \theta_0] \\
 \alpha_3 &= \frac{1}{3}\alpha_1[(\theta_U - \theta_0)^2 + (\theta_L - \theta_0)^2 + (\theta_U - \theta_0)(\theta_L - \theta_0)], \tag{11}
 \end{aligned}$$

Considering that the real DOA  $\theta_0$  is near the center of the integral intervals, we have  $\theta_0 \approx (\theta_U + \theta_L)/2$  and  $\theta_U - \theta_0 \approx \theta_L - \theta_0 \approx (\theta_U - \theta_L)/2$ . Then, we can then obtain the following equation:

$$\alpha_1 = \theta_U - \theta_L, \alpha_2 \approx 0, \alpha_3 = \frac{1}{4}\alpha_1^3. \tag{12}$$

According to (8), the matrix  $\mathbf{\Gamma}$  can be computed as follows:

$$\begin{aligned}
 \mathbf{\Gamma} &\approx \alpha_1 \sum_{m=1}^{M-K} \text{diag}\{\mathbf{b}_m\} \mathbf{a}_0^* \mathbf{a}_0^T \text{diag}^H\{\mathbf{b}_m\} \\
 &\quad + \frac{1}{4}\alpha_1^3 \sum_{m=1}^{M-K} \text{diag}\{\mathbf{b}_m\} [\mathbf{a}_0^* \mathbf{D}_2^T + \mathbf{D}_1^* \mathbf{D}_1^T + \mathbf{D}_2^* \mathbf{a}_0^T] \text{diag}^H\{\mathbf{b}_m\} \\
 &= \alpha_1 \text{diag}^H\{\mathbf{a}_0\} \left( \sum_{m=1}^{M-K} \mathbf{b}_m \mathbf{b}_m^H \right) \text{diag}\{\mathbf{a}_0\} \\
 &\quad + \frac{1}{4}\alpha_1^3 \sum_{m=1}^{M-K} \text{diag}\{\mathbf{b}_m\} [\mathbf{a}_0^* \mathbf{D}_2^T + \mathbf{D}_1^* \mathbf{D}_1^T + \mathbf{D}_2^* \mathbf{a}_0^T] \text{diag}^H\{\mathbf{b}_m\} \tag{13}
 \end{aligned}$$

Neglecting the scale factor in (13), which does not affect the result in (7), we obtain the following equation:

$$\mathbf{\Gamma} \approx \bar{\mathbf{\Gamma}} + \tilde{\mathbf{\Gamma}}, \tag{14}$$

where  $\bar{\mathbf{\Gamma}} = \text{diag}^H\{\mathbf{a}_0\} \left( \sum_{m=1}^{M-K} \mathbf{b}_m \mathbf{b}_m^H \right) \text{diag}\{\mathbf{a}_0\}$ , which is calculated by the precise DOA information, and  $\tilde{\mathbf{\Gamma}} = \frac{1}{4}\alpha_1^2 \sum_{m=1}^{M-K} \text{diag}\{\mathbf{b}_m\} [\mathbf{a}_0^* \mathbf{D}_2^T + \mathbf{D}_1^* \mathbf{D}_1^T + \mathbf{D}_2^* \mathbf{a}_0^T] \text{diag}^H\{\mathbf{b}_m\}$ . If the value of  $\theta_U - \theta_L$  is small, then  $\tilde{\mathbf{\Gamma}}$  is a small quantity of the second order of  $\theta_U - \theta_L$ , which can be approximately omitted. However, when the  $\theta_U - \theta_L$  value increases, the perturbation term  $\tilde{\mathbf{\Gamma}}$  should not be ignored, and the performance of the self-calibration algorithm in (5) degrades.

### 3.3 Refinement of DOA Estimation

A refinement operation is considered to boost the accuracy of the DOA and sensor gain and phase parameter estimation. The sensor gain and phase parameters estimated by (7) can be regarded as a reliable initial value of the iterative refinement operations.

The sensor gain and phase parameters at the  $i$ th iteration are calculated by the following cost function:

$$\min_{\boldsymbol{\gamma}} J = \min_{\boldsymbol{\gamma}} \boldsymbol{\gamma}^H \left( \sum_{k=1}^K \text{diag}^H\{\mathbf{a}(\hat{\theta}_k^{(i)})\} \Pi_{\mathbf{B}_s} \text{diag}\{\mathbf{a}(\hat{\theta}_k^{(i)})\} \right) \boldsymbol{\gamma}$$

**Table 1** Summary of estimation procedure

*Steps: initialization*

1	Give the rough regions of sources $\Theta = \bigcup_{k=1}^K [\theta_k, L, \theta_k, U]$
2	Set $i = 0$ and $\varepsilon = 0.0001$
3	Calculate matrix $\mathbf{\Gamma}$ in (6)
4	Compute $\hat{\mathbf{y}}^{(0)} = \mathbf{\Gamma}^{-1} \mathbf{e}_1 / (\mathbf{e}_1^H \mathbf{\Gamma}^{-1} \mathbf{e}_1)$
<i>Iteration</i>	
5	Estimate spatial spectrum in (17) and get $\hat{\theta}_k^{(i)}, k = 1, 2, \dots, K$
6	Compute $\hat{\mathbf{y}}^{(i)}$ in (16)
7	If $ J^{(i+1)} - J^{(i)} ^2 > \varepsilon$ , then set $i = i + 1$ and go to step 5
8	Obtain $\hat{\theta}_k^{(I)}$ and $\hat{\mathbf{y}}^{(I)}$ , respectively, where $I$ is the final iteration number

$$\text{s.t. } \mathbf{e}_1^H \mathbf{y} = 1, \tag{15}$$

where  $\hat{\theta}_k^{(i)}$  is the estimated direction of the  $k$ th source at the  $i$ th iteration. The optimal solution of the above problem is calculated as follows:

$$\hat{\mathbf{y}}^{(i)} = \mathbf{U}^{-1} \mathbf{e}_1 / (\mathbf{e}_1^H \mathbf{U}^{-1} \mathbf{e}_1)$$

$$\mathbf{U} = \sum_{k=1}^K \text{diag}^H\{\mathbf{a}(\hat{\theta}_k^{(i)})\} \Pi_{B_s} \text{diag}\{\mathbf{a}(\hat{\theta}_k^{(i)})\}. \tag{16}$$

Then, the DOA at the  $(i + 1)$ th iteration is estimated from the MUSIC spectrum:

$$P(\theta) = \frac{1}{\mathbf{a}^H(\theta) \text{diag}^H\{\hat{\mathbf{y}}^{(i)}\} \Pi_{B_s} \text{diag}\{\hat{\mathbf{y}}^{(i)}\} \mathbf{a}(\theta)}. \tag{17}$$

Similarly, the root-MUSIC-like method [13] can be also used to estimate DOA efficiently if the array is a uniform linear array (ULA). When  $i = 0$ , the initial value  $\hat{\mathbf{y}}^{(0)}$  is calculated by (7). Finally, the DOAs and the sensor gain and phase parameters are estimated alternately until convergence.

The iteration is terminated when the relative change  $|J^{(i+1)} - J^{(i)}|^2$  of the cost function in (15) at the  $(i + 1)$ th iteration is less than a specified tolerance  $\varepsilon$  or when the iteration number meets a fixed upper limit. An typical value of  $\varepsilon$  is 0.0001. Then, the proposed estimator for self-calibration is summarized in Table 1.

### 3.4 Computational Complexities and CRBs

*Complexities:* According to (6) and (7), the computational complexity of the initial sensor parameter estimation is  $O(M^2 K S)$ , where  $K$  is the number of sources,  $S$  is the number of discrete directions in the rough intervals, and  $K S$  is generally larger than  $M$ .

**Table 2** Sensor gain and phase parameters

Sensor	Gain	Phase (°)	Sensor	Gain	Phase (°)
1#	1	0	6#	1.0408	−24.5838
2#	1	0	7#	0.5651	−8.9654
3#	0.6433	−3.3855	8#	0.7678	−16.1294
4#	1.3298	3.7199	9#	0.8558	−26.1513
5#	0.8144	18.2121	10#	0.5537	14.1120

Then the iterative refinement operations have a complexity of  $O(M^3I)$ , where  $I$  is the final iteration number. Consequently, the algorithmic complexity is  $O(\max(M^2KS, M^3I))$ .

**CRBs:** The CRBs of DOA and unknown sensor gain and phase are derived in the references [8, 23] under a uniform noise model. In the present work, the CRBs are generalized to a non-uniform noise model. The detailed derivations are shown in Appendix.

## 4 Simulation Results

In this section, the performances of the proposed method and other self-calibration methods are compared. A uniform linear array with 10 sensors and a half-wavelength inter-element spacing is considered. The power of non-uniform noise is assumed as  $\sigma = [1, 2, 3, 4, 5, 6, 7, 8, 9, 10]^T$ . Then, unknown gain and phase parameters are randomly generated from uniform distributions  $g_m \sim U[0.5, 1.5]$  and  $\phi_m \sim U[-30^\circ, 30^\circ]$ , respectively; they are listed in Table 2. The symbol  $U[a, b]$  denotes a uniform distribution on the interval  $[a, b]$ .

### 4.1 Example I

The spatial spectrum of the proposed method is compared with those of the CBF method, ESPRIT-like algorithm, and MUSIC algorithm without calibration in this example. The ESPRIT-like algorithm and the MUSIC algorithm both utilize the signal subspace under the non-uniform noise model estimated by the iterative method proposed in the [10] instead of the principal eigenvectors of the sample covariance matrix. Three uncorrelated narrowband sources with the same power impinge on the array from the directions of  $-30^\circ$ ,  $0^\circ$ , and  $5^\circ$ . The signal-to-noise ratio (SNR) is the ratio of each source power to the average noise power, as follows:



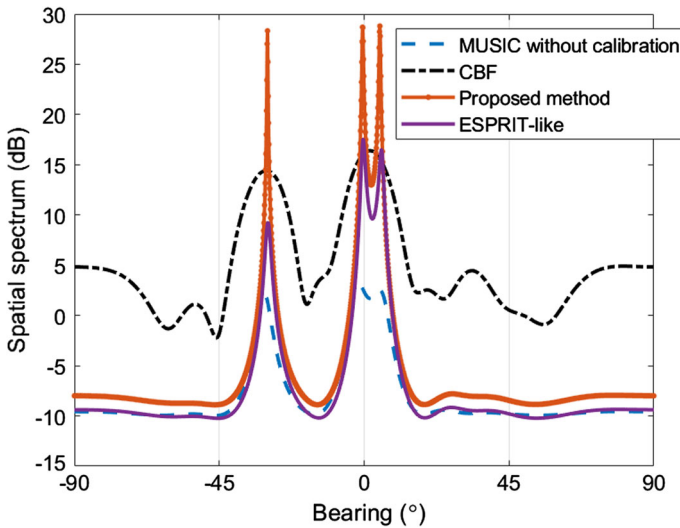


Fig. 1 Spatial spectra

$$SNR = \frac{1}{M} \sum_{m=1}^M \frac{p_s}{\sigma_m}, \tag{18}$$

where  $p_s$  is the signal power, and  $\sigma_m$  indicates the noise power in the  $m$ th sensor.

In this example, the SNR is set to 10 dB, and the number of snapshots is  $N = 200$ . The first  $M_c = 2$  sensors are calibrated well for the ESPRIT-like algorithm. Therefore, the complex responses of the first two sensors are set to 1, that is,  $\gamma_1 = \gamma_2 = 1$ . However, only the condition in which  $\gamma_1 = 1$  is needed for unique identification in the proposed method.

The spatial spectra of the proposed method, ESPRIT-like algorithm, MUSIC algorithm without calibration, and CBF are displayed in Fig. 1. The MUSIC algorithm without calibration has poor precision in DOA estimation and shows a low spatial resolution, particularly for close-spaced sources. The CBF as a low-resolution and robust direction-finding method is utilized to obtain the rough space intervals of sources selected as  $[-35^\circ, -24^\circ] \cup [-4^\circ, 9^\circ]$  according to the 3 dB beamwidth of the CBF beam pattern. Considering the advantages of calibrated parameters, the proposed method and ESPRIT-like algorithm both obtain high-resolution abilities. The statistical performances of the two methods are compared in the following examples.

### 4.2 Example II

The estimation performances of DOA and sensor responses are analyzed in this example. Three uncorrelated narrowband sources impinge on the test array from the directions of  $-20^\circ, 0^\circ$ , and  $20^\circ$ . The rough intervals of the sources in the proposed

method are chosen as  $\Theta = \bigcup_{k=1}^3 [\theta_k - \Delta\theta, \theta_k + \Delta\theta]$ , where the parameter  $\Delta\theta$  is set as  $5^\circ$ . The first two sensors are well pre-calibrated for the ESPRIT-like algorithm.

The performance of DOA estimation is measured by the root mean square error (RMSE), which is calculated as follows:

$$\text{RMSE}_\theta = \left( \frac{1}{KL} \sum_{l=1}^L \sum_{k=1}^K (\hat{\theta}_{k,l} - \theta_k)^2 \right)^{\frac{1}{2}}, \quad (19)$$

where  $K$  is the number of sources and is equal to three in this example,  $\hat{\theta}_{k,n}$  is the estimated direction of the  $k$ th source at the  $l$ th experiment, and  $L$  denotes the total number of Monte Carlo experiments. The RMSE of DOA in (19) is the average value of the  $K$  sources [7, 8, 19, 20]. Meanwhile, the estimates of the  $m$ th sensor gain and phase are measured as follows:

$$\text{RMSE}_{\varphi_m} = \left( \frac{1}{L} \sum_{l=1}^L (\hat{\varphi}_{m,l} - \varphi_m)^2 \right)^{\frac{1}{2}}, \quad (20)$$

and

$$\text{RMSE}_{g_m} = \left( \frac{1}{L} \sum_{l=1}^L (\hat{g}_{m,l} - g_m)^2 \right)^{\frac{1}{2}}, \quad (21)$$

where  $\hat{g}_{m,l}$  and  $\hat{\varphi}_{m,l}$  are the estimated sensor gain and phase of the  $m$ th sensor at the  $l$ th experiment, respectively.

A total of 200 Monte Carlo experiments are conducted at each SNR with the number of snapshots  $N = 200$ . The RMSE of DOA estimation versus SNR is shown in Fig. 2. The method in [29] which is the initial iteration result of the proposed method obtained from (7) has the poorest performance among the results due to the large rough interval parameter  $\Delta\theta$ . The whole array aperture is not fully utilized by the ESPRIT-like algorithm. Hence, the RMSE of ESPRIT-like algorithm is higher than that of the proposed method, whereas the proposed method exhibits an evident performance improvement and its RMSE is close to the CRB.

The estimation performances of sensor gain and phase are also analyzed in this example. Without loss of generality, the gain and phase estimations of the 4th, 7th and 10th sensors versus the SNR levels are shown in Figs. 3 and 4, respectively. The last subfigures in Figs. 3 and 4 show the average RMSE values over the uncalibrated sensors. The proposed method keeps a stable RMSE values for different sensors, while those of the compared methods have wide variances along the sensors. CRB is also approached by the proposed method for the 4th, 7th, and 10th sensors, especially at high SNR levels. According to the average RMSE values, the proposed method shows a remarkable performance improvement relative to the other methods.

Then, the estimation performances of the methods are evaluated in terms of the RMSE values versus the number of snapshots. Similarly, 200 Monte Carlo experiments

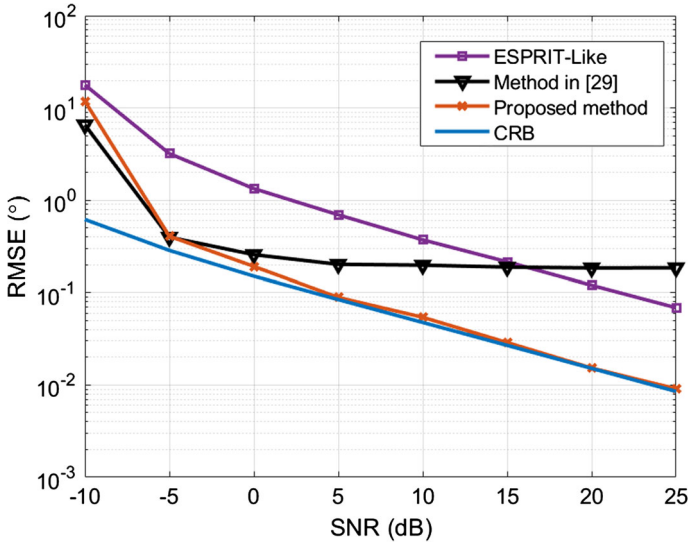


**Fig. 2** RMSE of DOA estimation versus SNR (DOA of sources:  $[-20^\circ, 0^\circ, 20^\circ]$ , the number of snapshots is 200)

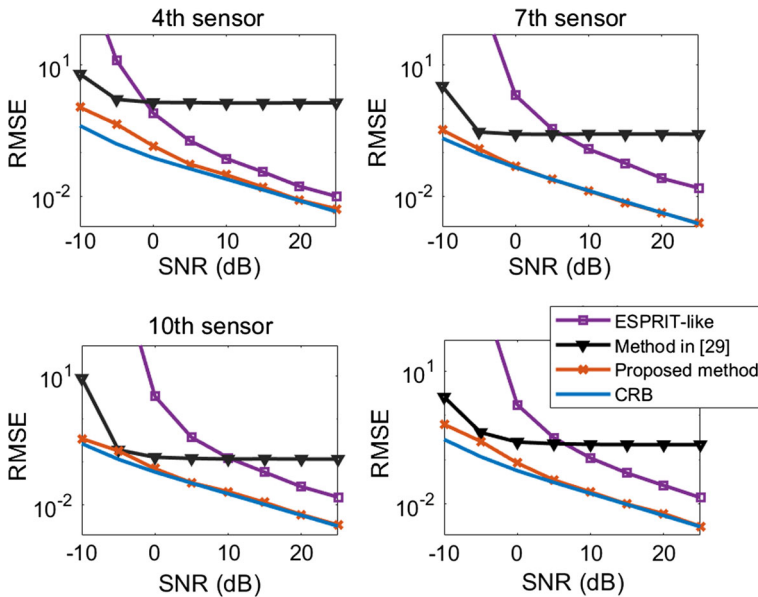


**Fig. 3** RMSE of sensor gain estimation versus SNR (DOA of sources:  $[-20^\circ, 0^\circ, 20^\circ]$ , the number of snapshots is 200)

are operated in every snapshot, which ranges from 10 to 200 in a step of 10 with SNR = 10 dB. The RMSEs of the DOA, the sensor gain, and the sensor phase versus the number of snapshots are plotted in Figs. 5, 6, and 7, respectively. Similarly, the proposed method obtains the best performance with the CRB well approached.

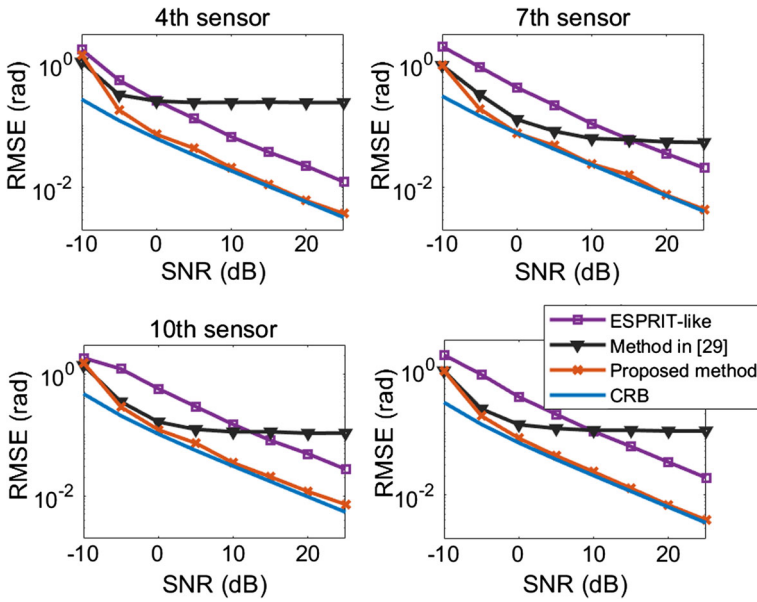


Fig. 4 RMSE of sensor phase estimation versus SNR (DOA of sources:  $[-20^\circ, 0^\circ, 20^\circ]$ , the number of snapshots is 200)

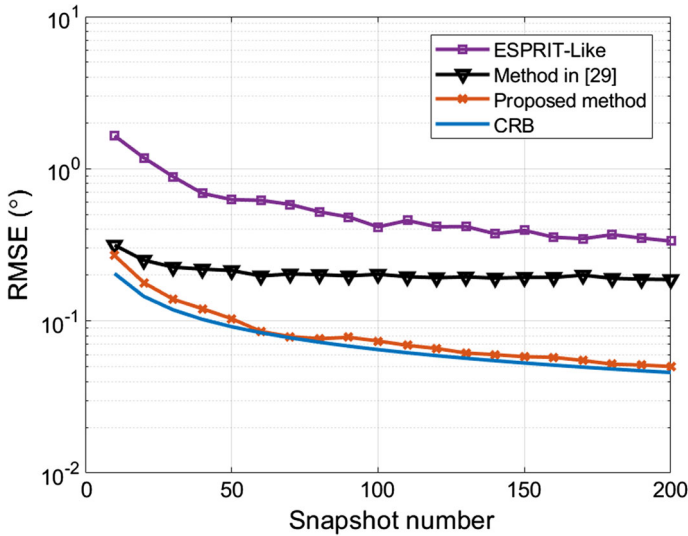


Fig. 5 RMSE of DOA estimation versus the number of snapshots (DOA of sources:  $[-20^\circ, 0^\circ, 20^\circ]$ , SNR = 10 dB)

In this simulation, the performance of the proposed method is compared in different non-uniform noise environments. We assume that the noise power of each sensor increases linearly between 1 and  $\sigma_{\max}$ , i.e., the noise power of the  $m$ th sensor  $\sigma_m =$

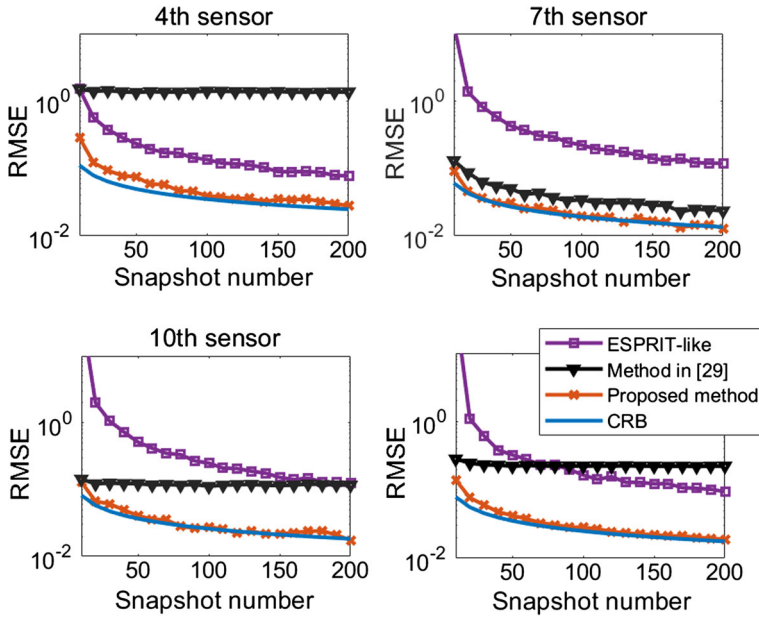


Fig. 6 RMSE of sensor gain estimation versus the number of snapshots (DOA of sources:  $[-20^\circ, 0^\circ, 20^\circ]$ , SNR = 10 dB)

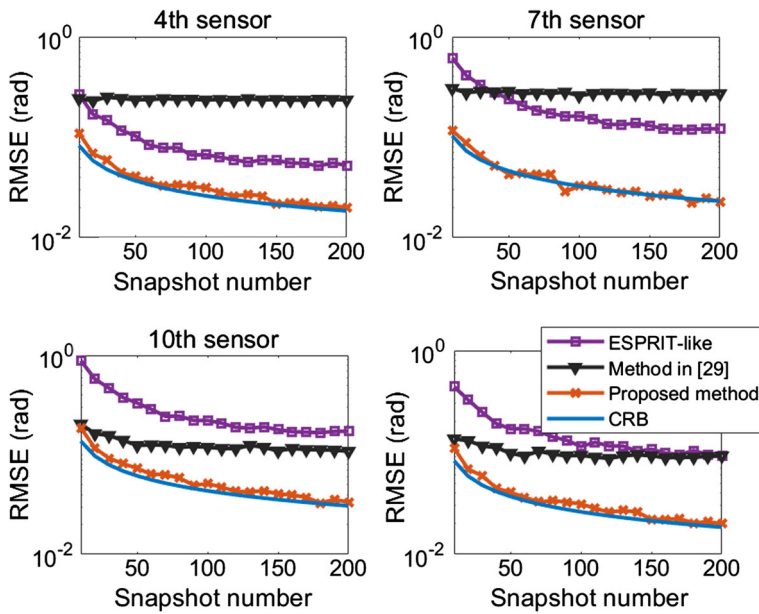
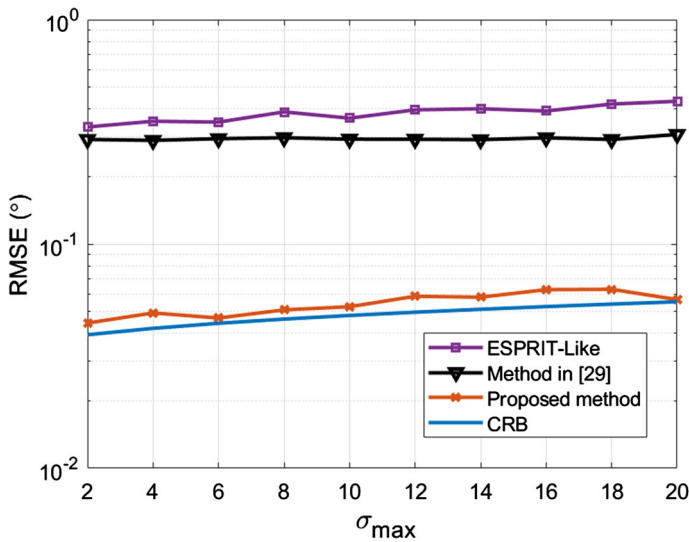


Fig. 7 RMSE of sensor phase estimation versus the number of snapshots (DOA of sources:  $[-20^\circ, 0^\circ, 20^\circ]$ , SNR = 10 dB)



**Fig. 8** RMSE of DOA estimation versus the maximum value of non-uniform noise power (DOA of sources:  $[-20^\circ, 0^\circ, 20^\circ]$ , SNR = 10 dB, the number of snapshots is 200)

$1 + (\sigma_{\max} - 1)(m - 1) / (M - 1)$ , where  $\sigma_{\max}$  varies from 2 to 20. The SNR is fixed at 10 dB, and 200 snapshots are available.

The RMSEs of the DOA, the sensor gain, and the sensor phase versus the maximum value of non-uniform noise power, i.e.,  $\sigma_{\max}$ , are plotted in Figs. 8, 9, and 10, respectively. The proposed method is robust to the non-uniform noise environment and has a lower RMSE than in the compared methods. The CRBs in Figs. 8, 9, and 10 all slightly increase with an increase in the non-uniformity of noise powers. They are well approached by the proposed method.

## 5 Experimental Results

To confirm the effectiveness of the proposed method further, we perform an experiment by using a 12-hydrophone baffled UCA with a radius of 0.24 m (Fig. 11). The experiment is performed in an anechoic tank. The geometric layout of the experiment is plotted in Fig. 12. Two narrowband sources with a center frequency of 5.7 kHz are sent by acoustic transducers, which are placed symmetrically along the  $x$ -axis. Note that the distance between the source and UCA is larger than  $2\Delta^2/\lambda$  [5], where the aperture of the UCA  $\Delta$  is 0.48 m and the wavelength  $\lambda$  is about 0.26 m. The acoustic transducers are thus located in the far field of the UCA.

### 5.1 Experiment with a Single Source

First, source 1 is enabled, and the waveforms of all the hydrophones are plotted in Fig. 13a. As a result of the shielding effect of the baffle, the amplitudes vary along

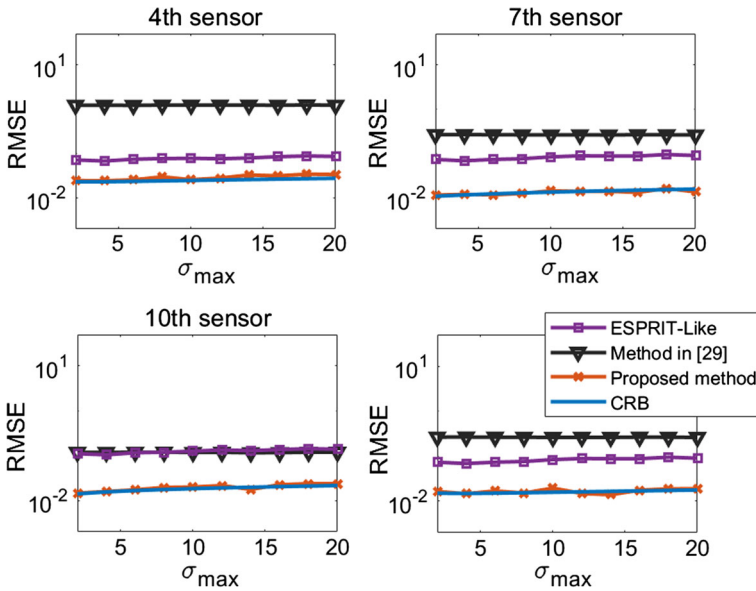


**Fig. 9** RMSE of sensor gain estimation versus the maximum value of non-uniform noise power (DOA of sources:  $[-20^\circ, 0^\circ, 20^\circ]$ , SNR = 10 dB, the number of snapshots is 200)

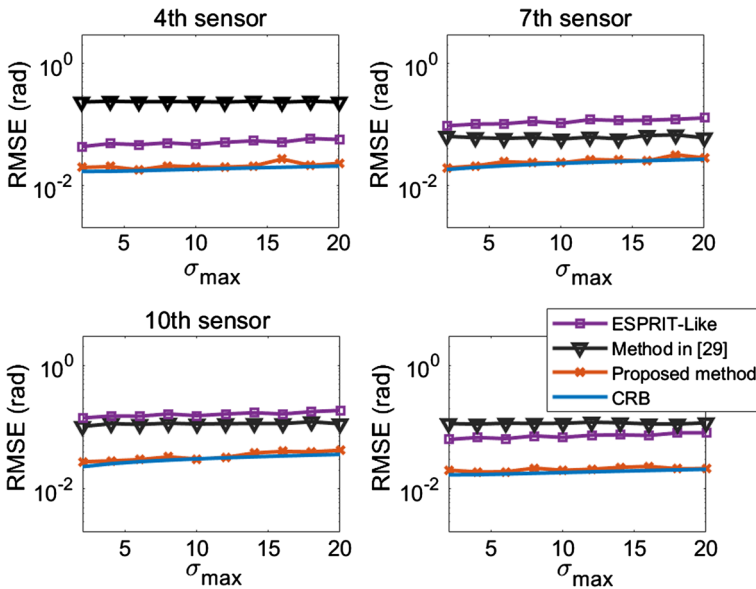


**Fig. 10** RMSE of sensor phase estimation versus the maximum value of non-uniform noise power (DOA of sources:  $[-20^\circ, 0^\circ, 20^\circ]$ , SNR = 10 dB, the number of snapshots is 200)

the array. The #1 and #8–#12 hydrophones are assembled on the back of the baffle. Therefore, the amplitudes are smaller than the others.

Fig. 11 Experimental UCA

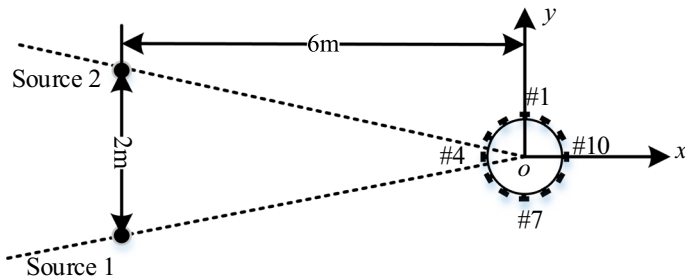


Fig. 12 Geometric layout of the experiment

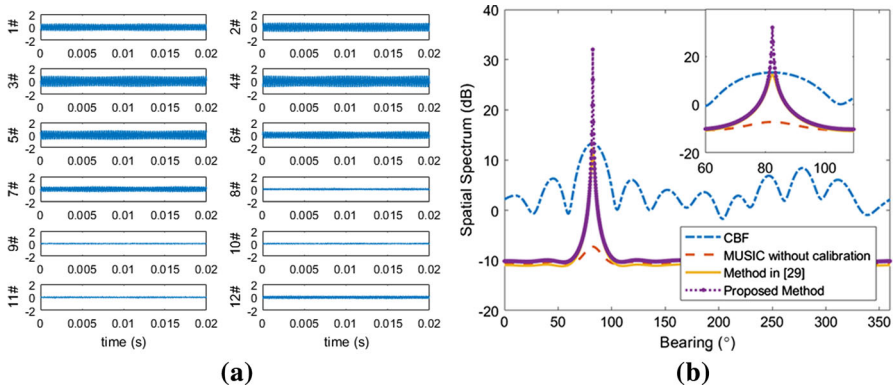


Fig. 13 Experimental results of source 1. **a** Waveforms of 12 hydrophones and **b** spatial spectra

The spatial spectrum of the proposed method relative to those of the CBF, MUSIC without calibration, and calibration method in [29] is displayed in Fig. 13b. The performance of the MUSIC algorithm without calibration degrades rapidly due to the uncertainties of the sensor gain and phase responses, whereas the spatial spectra of the calibration method in [29] and the proposed method are both significantly improved. An extremely sharp peak corresponding to the correct location of the transducer is obtained in the spatial spectrum of the proposed method. The estimated sensor gain



**Table 3** Sensor gain and phase parameter estimation with enabled source 1

Sensor	Gain	Phase (°)	Sensor	Gain	Phase (°)
1#	1.0000	0.0000	7#	0.7797	−9.9895
2#	1.2710	14.1105	8#	0.2924	−11.9459
3#	1.4679	13.1076	9#	0.1741	−47.5814
4#	1.5564	19.5110	10#	0.1746	28.1377
5#	1.2932	16.7338	11#	0.1933	−20.5763
6#	1.0556	8.4812	12#	0.4380	0.1113

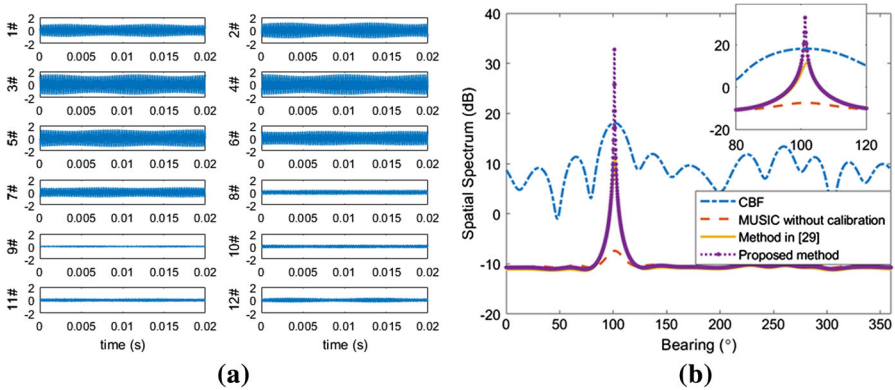


**Fig. 14** Experimental results of source 2. **a** Waveforms of 12 hydrophones and **b** spatial spectra

**Table 4** Sensor gain and phase parameter estimation with enabled source 2

Sensor	Gain	Phase (°)	Sensor	Gain	Phase (°)
1#	1.0000	0.0000	7#	0.8529	−5.0178
2#	1.2271	7.1686	8#	0.3435	−8.9898
3#	1.4940	20.4633	9#	0.1808	−32.9589
4#	1.5848	27.2291	10#	0.2612	30.9571
5#	1.3890	23.9615	11#	0.2591	−28.9373
6#	1.1678	19.0935	12#	0.3511	−2.9820

and phase parameters are listed in Table 3. The estimated gain responses of all the hydrophones conform to the amplitude of the waveforms displayed in Fig. 13a.

The waveform and spatial spectrum for source 2 are displayed in Fig. 14a, b, respectively. The proposed method achieves the best DOA estimation performance among the compared methods. The estimated sensor gain and phase parameters are listed in Table 4. The values of the estimated gain parameters are similar to the amplitudes of the received waveforms.

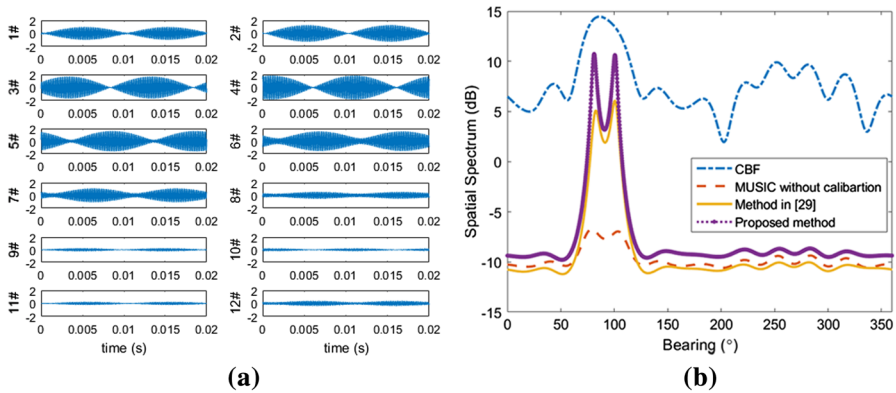


Fig. 15 Experimental results for double sound sources. **a** Waveforms of 12 hydrophones and **b** spatial spectra

### 5.2 Experiment with Double Sources

In this situation, sources 1 and 2 are enabled separately. The sample covariance matrices of the two sources, i.e.,  $\hat{\mathbf{R}}_1$  and  $\hat{\mathbf{R}}_2$ , can be calculated, respectively. Then the covariance matrix of the double sources can be equivalently calculated by summing  $\hat{\mathbf{R}}_1$  and  $\hat{\mathbf{R}}_2$ . This is because that

$$\begin{aligned}
 \mathbf{R}_1 &= p_1 \mathbf{a}_1 \mathbf{a}_1^H + \text{diag}\{\boldsymbol{\sigma}\} \\
 \mathbf{R}_2 &= p_2 \mathbf{a}_2 \mathbf{a}_2^H + \text{diag}\{\boldsymbol{\sigma}\} \\
 \mathbf{R}_1 + \mathbf{R}_2 &= p_1 \mathbf{a}_1 \mathbf{a}_1^H + p_2 \mathbf{a}_2 \mathbf{a}_2^H + \text{diag}\{2\boldsymbol{\sigma}\} \\
 &= [\mathbf{a}_1 \ \mathbf{a}_2] \begin{bmatrix} p_1 & 0 \\ 0 & p_2 \end{bmatrix} [\mathbf{a}_1 \ \mathbf{a}_2]^H + \text{diag}\{2\boldsymbol{\sigma}\}, \tag{22}
 \end{aligned}$$

where  $\mathbf{R}_1$  and  $\mathbf{R}_2$  are the covariance matrix of sources 1 and 2, respectively;  $\mathbf{a}_1$  and  $\mathbf{a}_2$  are the steering vector of sources 1 and 2, respectively; and  $p_1$ ,  $p_2$  and  $\boldsymbol{\sigma}$  are the power of source 1, source 2, and noise, respectively. In this manner, the covariance matrix of two incoherent narrowband signals is obtained.

The superimposed waveforms of sources 1 and 2 are shown in Fig. 15a. After calibrating the gain and phase responses of each hydrophone, we observe a significant improvement in the performances of the method in [29] and the proposed method, as shown in Fig. 15b. The proposed method utilizes an iterative scheme to improve the estimates of the sensor gain and phase and the estimation results are listed in Table 5. Due to the accurate calibrations of the sensor responses, a high resolution of DOA estimation can be obtained by the proposed method.

### 6 Conclusions

A robust direction-finding method for uncalibrated arrays is presented. This method is a robust estimator of unknown parameters, namely DOAs, sensor gains, and sensor

**Table 5** Sensor gain and phase parameter estimation with double sources

Sensor	Gain	Phase (°)	Sensor	Gain	Phase (°)
1#	1.0000	0.0000	7#	0.8295	−0.4820
2#	1.1141	9.5137	8#	0.4217	−8.4875
3#	1.4285	12.4347	9#	0.1685	−29.5559
4#	1.4877	17.2260	10#	0.2048	63.1107
5#	1.2676	18.3475	11#	0.2078	−28.5719
6#	1.1360	18.9718	12#	0.3227	−12.0880

phases. The initial iteration step of the proposed method is generally polluted by the perturbation matrix  $\tilde{\mathbf{T}}$  in (14), which degrades the estimation performance particularly for the large ranges of rough intervals. Therefore, an iterative operation is carried out to improve the accuracy of the estimation of DOA and sensor parameters. The proposed method does not require a specific array structure or partly calibrated sensors.

The influence of the range of rough intervals is analyzed, and the CRBs with unknown sensor gains and phases in the non-uniform noise model are derived. The simulation results show that the proposed method can achieve excellent statistical performance and is robust to the selection of the range of initial rough regions. The effectiveness of the proposed method is also confirmed by experimental results in an anechoic tank with a baffled UCA.

**Acknowledgements** This work was supported in part by the National Natural Science Foundation of China under Grants 11527809, 11604259, and 51679204, and in part by the China Postdoctoral Science Foundation under Grant 2019M653569.

### Appendix: The CRB in the Non-uniform Noise Environment

In this appendix, the CRB under the non-uniform noise is calculated. The parameter vector containing all unknown parameters is

$$\mathbf{z} = [\boldsymbol{\theta}^T, \mathbf{g}^T, \boldsymbol{\varphi}^T, \mathbf{p}^T, \boldsymbol{\sigma}^T]^T, \tag{23}$$

where  $\boldsymbol{\theta} = [\theta_1, \theta_2, \dots, \theta_K]^T$  is the direction of sources;  $\mathbf{g}$ ,  $\boldsymbol{\varphi}$ , and  $\mathbf{p}$  are the sensor gains, phases, and signal powers, respectively; and  $\boldsymbol{\sigma} = [\sigma_1, \sigma_2, \dots, \sigma_M]^T$  includes the noise powers of each sensor.

When  $N$  independent samples of a zero-mean Gaussian process is given, the CRB equals the inverse of the Fisher information matrix (FIM) whose  $(m, n)$ th entry is given by

$$\mathbf{F}_{mn} = N \times \text{tr} \left\{ \mathbf{R}^{-1} \frac{\partial \mathbf{R}}{\partial z_m} \mathbf{R}^{-1} \frac{\partial \mathbf{R}}{\partial z_n} \right\}, \tag{24}$$

where  $\text{tr}\{\cdot\}$  denotes the trace operator and  $\mathbf{R}$  is defined in (3). Then, the FIM can be expressed as a block matrix:

$$\mathbf{F} = \begin{bmatrix} \mathbf{F}_{\theta\theta} & \mathbf{F}_{\theta g} & \mathbf{F}_{\theta\varphi} & \mathbf{F}_{\theta p} & \mathbf{F}_{\theta\sigma} \\ \mathbf{F}_{\theta g}^T & \mathbf{F}_{gg} & \mathbf{F}_{g\varphi} & \mathbf{F}_{gp} & \mathbf{F}_{g\sigma} \\ \mathbf{F}_{\theta\varphi}^T & \mathbf{F}_{g\varphi}^T & \mathbf{F}_{\varphi\varphi} & \mathbf{F}_{\varphi p} & \mathbf{F}_{\varphi\sigma} \\ \mathbf{F}_{\theta p}^T & \mathbf{F}_{gp}^T & \mathbf{F}_{\varphi p}^T & \mathbf{F}_{pp} & \mathbf{F}_{p\sigma} \\ \mathbf{F}_{\theta\sigma}^T & \mathbf{F}_{g\sigma}^T & \mathbf{F}_{\varphi\sigma}^T & \mathbf{F}_{p\sigma}^T & \mathbf{F}_{\sigma\sigma} \end{bmatrix}. \quad (25)$$

First, we define the matrices  $\dot{\bar{\mathbf{A}}}_\theta$ ,  $\dot{\bar{\mathbf{A}}}_g$ , and  $\dot{\bar{\mathbf{A}}}_\varphi$  as

$$\dot{\bar{\mathbf{A}}}_\theta = \sum_{k=1}^K \frac{\partial \bar{\mathbf{A}}}{\partial \theta_k}, \dot{\bar{\mathbf{A}}}_g = \sum_{m=1}^M \frac{\partial \bar{\mathbf{A}}}{\partial g_m}, \dot{\bar{\mathbf{A}}}_\varphi = \sum_{m=1}^M \frac{\partial \bar{\mathbf{A}}}{\partial \varphi_m}, \quad (26)$$

where  $\bar{\mathbf{A}} = \text{diag}\{\boldsymbol{\gamma}\}\mathbf{A}$  is the real steering vector and  $\mathbf{A}$  is the nominal steering vector. A  $(M - M_c) \times M$  selection matrix  $\mathbf{H}$  is constituted by  $\mathbf{I}$  rows of the identity matrix; the set  $\mathbf{I}$  contains  $M - M_c$  uncalibrated sensors.

In consideration of the non-uniform noise model, the last column of the block matrices should be recalculated, and the other blocks remain unchanged, such as that in [8] and [23].

According to (3), we have

$$\frac{\partial \mathbf{R}}{\partial \boldsymbol{\theta}_p} = \dot{\bar{\mathbf{A}}}_\theta \mathbf{e}_p \mathbf{e}_p^T \mathbf{P} \mathbf{A}^H + \mathbf{A} \mathbf{P} \mathbf{e}_p \mathbf{e}_p^T \dot{\bar{\mathbf{A}}}_\theta^H, \quad (27a)$$

$$\frac{\partial \mathbf{R}}{\partial \mathbf{g}_p} = \mathbf{e}_p \mathbf{e}_p^T \dot{\bar{\mathbf{A}}}_g \mathbf{P} \mathbf{A}^H + \mathbf{A} \mathbf{P} \dot{\bar{\mathbf{A}}}_g^H \mathbf{e}_p \mathbf{e}_p^T, \quad (27b)$$

$$\frac{\partial \mathbf{R}}{\partial \boldsymbol{\varphi}_p} = \mathbf{e}_p \mathbf{e}_p^T \dot{\bar{\mathbf{A}}}_\varphi \mathbf{P} \mathbf{A}^H + \mathbf{A} \mathbf{P} \dot{\bar{\mathbf{A}}}_\varphi^H \mathbf{e}_p \mathbf{e}_p^T, \quad (27c)$$

$$\frac{\partial \mathbf{R}}{\partial \mathbf{p}_p} = \bar{\mathbf{A}} \mathbf{e}_p \mathbf{e}_p^T \bar{\mathbf{A}}^H, \quad (27d)$$

$$\frac{\partial \mathbf{R}}{\partial \boldsymbol{\sigma}_p} = \mathbf{e}_p \mathbf{e}_p^T, \quad (27e)$$

where  $\mathbf{e}_p$  is a vector with the  $p$ th element equal to 1 and the other equal to 0.

Substituting (27a)–(27e) into (24), we can, respectively, obtain  $\mathbf{F}_{\theta\sigma}$ ,  $\mathbf{F}_{g\sigma}$ ,  $\mathbf{F}_{\varphi\sigma}$ ,  $\mathbf{F}_{p\sigma}$ , and  $\mathbf{F}_{\sigma\sigma}$  as

$$F_{\theta\sigma} = 2\text{Re} \left\{ \left( P \bar{A}^H R^{-1} \right) \circ \left( R^{-1} \dot{\bar{A}}_\theta \right)^T \right\}, \quad (28a)$$

$$F_{g\sigma} = 2\text{Re} \left\{ H \left( \dot{\bar{A}}_g P \bar{A}^H R^{-1} \right) \circ \left( R^{-1} \right)^T \right\}, \quad (28b)$$

$$F_{\varphi\sigma} = 2\text{Re} \left\{ H \left( \dot{\bar{A}}_\varphi P \bar{A}^H R^{-1} \right) \circ \left( R^{-1} \right)^T \right\}, \quad (28c)$$

$$F_{p\sigma} = \left( \bar{A}^H R^{-1} \right) \circ \left( R^{-1} \bar{A} \right)^T, \quad (28d)$$

$$F_{\sigma\sigma} = \left( R^{-1} \right) \circ \left( R^{-1} \right)^T. \quad (28e)$$

The other block matrices of FIM are listed as follows:

$$F_{\theta\theta} = 2\text{Re} \left\{ \left( P \bar{A}^H R^{-1} \bar{A} P \right) \circ \left( \dot{\bar{A}}_\theta^H R^{-1} \dot{\bar{A}}_\theta \right)^T + \left( P \bar{A}^H R^{-1} \dot{\bar{A}}_\theta \right) \circ \left( P \bar{A}^H R^{-1} \dot{\bar{A}}_\theta \right)^T \right\},$$

$$F_{\theta g} = 2\text{Re} \left\{ \left[ \left( P \bar{A}^H R^{-1} \right) \circ \left( \dot{\bar{A}}_g P \bar{A}^H R^{-1} \dot{\bar{A}}_\theta \right)^T + \left( P \bar{A}^H R^{-1} \bar{A} P \dot{\bar{A}}_g^H \right) \circ \left( R^{-1} \dot{\bar{A}}_\theta \right)^T \right] H^T \right\},$$

$$F_{\theta\varphi} = 2\text{Re} \left\{ \left[ \left( P \bar{A}^H R^{-1} \right) \circ \left( \dot{\bar{A}}_\varphi P \bar{A}^H R^{-1} \dot{\bar{A}}_\theta \right)^T + \left( P \bar{A}^H R^{-1} \bar{A} P \dot{\bar{A}}_\varphi^H \right) \circ \left( R^{-1} \dot{\bar{A}}_\theta \right)^T \right] H^T \right\},$$

$$F_{\theta p} = 2\text{Re} \left\{ \left( P \bar{A}^H R^{-1} \bar{A} \right) \circ \left( \bar{A}^H R^{-1} \dot{\bar{A}}_\theta \right)^T \right\},$$

$$F_{g g} = 2\text{Re} \left\{ H \left[ \left( \dot{\bar{A}}_g P \bar{A}^H R^{-1} \right) \circ \left( \dot{\bar{A}}_g P \bar{A}^H R^{-1} \right)^T + \left( \dot{\bar{A}}_g P \bar{A}^H R^{-1} \bar{A} P \dot{\bar{A}}_g^H \right) \circ \left( R^{-1} \right)^T \right] H^T \right\},$$

$$F_{g\varphi} = 2\text{Re} \left\{ H \left[ \left( \dot{\bar{A}}_g P \bar{A}^H R^{-1} \right) \circ \left( \dot{\bar{A}}_\varphi P \bar{A}^H R^{-1} \right)^T + \left( \dot{\bar{A}}_\varphi P \bar{A}^H R^{-1} \bar{A} P \dot{\bar{A}}_g^H \right) \circ \left( R^{-1} \right)^T \right] H^T \right\},$$

$$F_{g p} = 2\text{Re} \left\{ H \left[ \left( \dot{\bar{A}}_g P \bar{A}^H R^{-1} \bar{A} \right) \circ \left( \bar{A}^H R^{-1} \right)^T \right] H^T \right\},$$

$$F_{\varphi\varphi} = 2\text{Re} \left\{ H \left[ \left( \dot{\bar{A}}_\varphi P \bar{A}^H R^{-1} \right) \circ \left( \dot{\bar{A}}_\varphi P \bar{A}^H R^{-1} \right)^T + \left( \dot{\bar{A}}_\varphi P \bar{A}^H R^{-1} \bar{A} P \dot{\bar{A}}_\varphi^H \right) \circ \left( R^{-1} \right)^T \right] H^T \right\},$$

$$F_{\varphi p} = 2\text{Re} \left\{ H \left[ \left( \dot{\bar{A}}_\varphi P \bar{A}^H R^{-1} \bar{A} \right) \circ \left( \bar{A}^H R^{-1} \right)^T \right] H^T \right\},$$

$$F_{p p} = \left( \bar{A}^H R^{-1} \bar{A} \right) \circ \left( \bar{A}^H R^{-1} \bar{A} \right)^T.$$

## References

1. D. Astély, A.L. Swindlehurst, B. Ottersten, Spatial signature estimation for uniform linear arrays with unknown receiver gains and phase. *IEEE Trans. Signal Process.* **47**(8), 2128–2138 (1999)
2. Q. Cheng, Y. Hua, P. Stoica, Asymptotic performance of optimal gain-and-phase estimators of sensor arrays. *IEEE Trans. Signal Process.* **48**(12), 3587–3590 (2000)
3. B.P. Flanagan, K.L. Bell, Array self-calibration with large sensor position errors. *Sig. Process.* **81**(10), 2201–2214 (2001)

4. Z. He, Z. Shi, L. Huang, Covariance sparsity-aware DOA estimation for nonuniform noise. *Digit. Signal Process.* **28**, 75–81 (2014)
5. R.C. Johnson, *Antenna engineering handbook*, 3rd edn. (McGraw-Hill, New York, 1993)
6. M. Li, Y. Lu, Source bearing and steering-vector estimation using partially calibrated arrays. *IEEE Trans. Aerosp. Electron. Syst.* **45**(4), 1361–1372 (2009)
7. B. Liao, S.C. Chan, Direction finding with partly calibrated uniform linear arrays. *IEEE Trans. Antennas Propag.* **60**(2), 922–929 (2012)
8. B. Liao, S.C. Chan, Direction finding in partly calibrated uniform linear arrays with unknown gains and phases. *IEEE Trans. Aerosp. Electron. Syst.* **51**(1), 217–227 (2015)
9. B. Liao, L. Huang, C. Guo, H.C. So, New approaches to direction-of-arrival estimation with sensor arrays in unknown nonuniform noise. *IEEE Sens. J.* **16**(24), 8982–8989 (2016)
10. B. Liao, S.C. Chan, L. Huang, C. Guo, Iterative methods for subspace and DOA estimation in nonuniform noise. *IEEE Trans. Signal Process.* **64**(12), 3008–3020 (2016)
11. C.S. MacInnes, Source localization using subspace estimation and spatial filtering. *IEEE J. Ocean. Eng.* **29**(2), 488–497 (2004)
12. M. Pesavento, A.B. Gershman, K.M. Wong, Direction finding in partly calibrated sensor arrays composed of multiple subarrays. *IEEE Trans. Signal Process.* **50**(9), 2103–2115 (2002)
13. B.D. Rao, K.V.S. Hari, Performance analysis of root-MUSIC. *IEEE Trans. Acoust. Speech Signal Process.* **37**(12), 1939–1949 (1989)
14. R. Roy, T. Kailath, ESPRIT-estimation of signal parameters via rotational invariance techniques. *IEEE Trans. Acoust. Speech Signal Process.* **37**(7), 984–995 (1989)
15. R. Schmidt, Multiple emitter location and signal parameter estimation. *IEEE Trans. Antennas Propag.* **34**(3), 276–280 (1986)
16. S.D. Somasundaram, N.H. Parsons, Evaluation of robust Capon beamforming for passive sonar. *IEEE J. Ocean. Eng.* **36**(4), 686–695 (2011)
17. K. Sun, Y. Liu, H. Meng, X. Wang, Adaptive sparse representation for source localization with gain/phase errors. *Sensors* **11**(5), 4780–4793 (2011)
18. M. Viberg, B. Ottersten, T. Kailath, Detection and estimation in sensor arrays using weighted subspace fitting. *IEEE Trans. Signal Process.* **39**(11), 2436–2449 (1991)
19. B. Wang, W. Wang, Y. Gu, S. Lei, Underdetermined DOA estimation of quasi-stationary signals using a partly-calibrated array. *Sensors* **17**(4), 702 (2017)
20. B. Wang, Y.D. Zhang, W. Wang, Robust DOA estimation in the presence of miscalibrated sensors. *IEEE Signal Proc. Lett.* **24**(7), 1073–1077 (2017)
21. M. Wang, Z. Zhang, A. Nehorai, Performance analysis of coarray-based MUSIC in the presence of sensor location errors. *IEEE Trans. Signal Process.* **66**(12), 3074–3085 (2018)
22. A.J. Weiss, B. Friedlander, Eigenstructure methods for direction finding with sensor gain and phase uncertainties. *Circuits Syst. Signal Process.* **9**(3), 271–300 (1990)
23. A.J. Weiss, B. Friedlander, DOA and steering vector estimation using a partially calibrated array. *IEEE Trans. Aerosp. Electron. Syst.* **32**(3), 1047–1057 (1996)
24. A.J. Weiss, B. Friedlander, “Almost blind” steering vector estimation using second-order moments. *IEEE Trans. Signal Process.* **44**(4), 1024–1027 (1996)
25. F. Wen, X. Zhang, Z. Zhang, CRBs for direction-of-departure and direction-of-arrival estimation in collocated MIMO radar in the presence of unknown spatially coloured noise. *IET Radar Sonar Nav.* **13**(4), 530–537 (2019)
26. M.P. Wylie, S. Roy, H. Messer, Joint DOA estimation and phase calibration of linear equispaced (LES) arrays. *IEEE Trans. Signal Process.* **42**(12), 3449–3459 (1994)
27. L. Yang, Y. Yang, Y. Wang, Sparse spatial spectral estimation in directional noise environment. *J. Acoust. Soc. Am.* **140**(3), EL263–EL268 (2016)
28. L. Yang, Y. Yang, J. Yang, Robust adaptive beamforming for uniform linear arrays with sensor gain and phase uncertainties. *IEEE Access* **7**, 2677–2685 (2019)
29. M. Zhang, Z. Zhu, A method for direction finding under sensor gain and phase uncertainties. *IEEE Trans. Antennas Propag.* **43**(8), 880–883 (1995)
30. X. Zhang, Z. He, B. Liao, X. Zhang, J. Xie, DOA and phase error estimation using one calibrated sensor in ULA. *Multidim. Syst. Sign. Proc.* **29**(2), 523–535 (2018)